SleepSense: A Noncontact and Cost-Effective Sleep Monitoring System

Feng Lin, *Member, IEEE*, Yan Zhuang, *Student Member, IEEE*, Chen Song, *Student Member, IEEE*, Aosen Wang, *Student Member, IEEE*, Yiran Li, *Student Member, IEEE*, Changzhan Gu, *Member, IEEE*, Changzhi Li, *Senior Member, IEEE*, and Wenyao Xu, *Member, IEEE*

***Abstract*—Quality of sleep is an important indicator of health and well being. Recent developments in the field of in-home sleep monitoring have the potential to enhance a person's sleeping experience and contribute to an overall sense of well being. Existing in-home sleep monitoring devices either fail to provide adequate sleep information or are obtrusive to use. To overcome these obstacles, a noncontact and cost-effective sleep monitoring system, named SleepSense, is proposed for continuous recognition of the sleep status, including on-bed movement, bed exit, and breathing section. SleepSense consists of three parts: a Doppler radar-based sensor, a robust automated radar demodulation module, and a sleep status recognition framework. Herein, several time-domain and frequency-domain features are extracted for the sleep recognition framework. A prototype of SleepSense is presented and evaluated using two sets of experiments. In the short-term controlled experiment, the SleepSense achieves an overall 95.1% accuracy rate in identifying various sleep status. In the 75-minute sleep study, SleepSense demonstrates wide usability in real life. The error rate for breathing rate extraction in this study is only 6.65%. These experimental results indicate that SleepSense is an effective and promising solution for in-home sleep monitoring.**

***Index Terms*—Evaluation, non-contact sensing, sleep monitoring.**

I. Introduction

QUALITY of sleep has a great impact on human health. There is a growing recognition of the adverse effects from poor sleep quality and sleep disorders. Patients with sleep disorders are prone to suffer from chronic diseases such as obesity, diabetes, and hypertension. Vorona *et al.* [2] demonstrated the relationship between obesity and sleep time. Spiegel *et al.* [3] showed that sleep loss increases the risk for diabetes and obesity. Brooks *et al.* [4] presented that obstructive sleep apnea (OSA) is a risk factor for systemic hypertension. Moreover, people are usually not aware of sleep disorders because they happen during sleep. It has became a chronic, under-explored but critical health challenge in modern life [5].

To date, there are several methods to perform sleep monitoring such as polysomnography (PSG) [6], ballistocardiogram [7], photoplethysmography [8] and actigraphy [9]. The PSG is still the primary and the most objective sleep assessment method in clinical use, such as insomnia diagnosis [10]. The PSG can provide fine-grained information for sleep monitoring, thus offering more accurate sleep assessment results. Another common alternative sleeping estimation method is actigraphy, including an accelerometer and a memory storage chip, which can provide information on movements during sleep [11]. Several commercial off-the-shelf (COTS) actigraphy based products, such as Sleep Tracker [12], Fitbit [13], and Sleep Cycle [14], are publicly available. The competitive advantage of this method is that it is convenient to deploy and inexpensive. Recent research suggests the need for new sleep monitoring approaches and methods. For example, Rofouei *et al.* [15] presented a non-invasive wearable neck-cuff system for sleep monitoring. The system can also visualize the physiological measurements in real time. Wang *et al.* [16] developed a real-time infrared-based video system to detect abnormal breathing pattern for diagnosis of sleep apnea. Hao *et al.* [17] presented a sleep quality monitoring system using an off-the-shelf smartphone. This lightweight system employs a built-in microphone and an accelerometer to determine sleep profiles. Liu *et al.* [18] designed a non-invasive pressure-sensitive bedsheet to monitor different sleep postures. The generated high-resolution pressure maps can be further utilized for sleep monitoring. Nevertheless, current monitoring methods suffer from several drawbacks, such as obtrusiveness [10], [15], lack of privacy [16], [17], and high-cost [10], [18]. These limitations prevent people from using current sleep monitoring systems on a daily basis.

To address the above challenges, we propose the SleepSense, a Doppler radar-based sleep monitoring system, which is non-contact and cost-effective. Our goal of this work is to monitor and classify the sleep-related events by detecting the on-bed movement activities during sleep based on the radar signal, without including sleep-wake classification. The Doppler radar sensor is a specialized radar that can measure target displacement remotely by using the Doppler effect [19] and has been employed in various motion detection applications, such as gait assessment, vital signal detection, human detection, and hand gesture recognition. Wang *et al.* [20] developed an in-home

Manuscript received June 17, 2015; revised November 8, 2015 and February 3, 2016; accepted March 7, 2016. Date of publication July 28, 2016; date of current version January 26, 2017. This work was supported in part by ECCS-1462498 and ECCS-1254838. An early version [1] was presented at IEEE Body Sensor Networks Conference 2015, Boston, MA, USA. This paper was recommended by Associate Editor S. Leonhardt.

F. Lin, Y. Zhuang, C. Song, A. Wang, and W. Xu are with the Department of Computer Science and Engineering, University at Buffalo, the State University of New York (SUNY), Buffalo, NY 14260 USA (e-mail: flin28@buffalo.edu; yanzhuan@buffalo.edu; csong5@buffalo.edu; aosenwan@buffalo.edu; wenyaoxu@buffalo.edu).

Y. Li, C. Gu, and C. Li are with the Department of Electrical and Computer Engineering, Texas Tech University, Lubbock, TX 79409 USA (e-mail: yiran.li@ttu.edu; changzhan.gu@ttu.edu; changzhi.li@ttu.edu).

Color versions of one or more of the figures in this paper are available online at http://ieeexplore.ieee.org.

Digital Object Identifier 10.1109/TBCAS.2016.2541680

gait assessment for older adults to reduce the fall risk based on Doppler radar. Lee *et al.* [21] demonstrated the capability of Doppler radar in capturing the breathing signals. Zheng *et al.* [22] proposed a Doppler radar-based hand gesture recognition system. Kim *et al.* [23] proposed a Doppler radar-based human detection system. Gu *et al.* [24] built a Doppler radar for noncontact vital sign detection. There also exist similar methods to Doppler radar by using ultrawideband (UWB) radar [25]–[27] for motion detection on the bed and for respiratory rate monitoring. In our study, we design and implement a Doppler radar sensor using commercial off-the-shelf (COTS) components, which are able to accurately capture the sleep-related signal. Then, the sampled baseband radar signal goes through a demodulation module that uses the extended differentiate and cross multiple (DACM) algorithm to obtain the body movement information from sleep status. Moreover, the sleep status recognition framework processes the displacement signal and recognizes three sleep status[1] stages, i.e., on-bed movement, bed exit, and breathing section. Meanwhile, the breathing rate is extracted via a novel breathing rate extracting algorithm. Finally, the system is evaluated by a set of real-case studies. Specifically, in our short-term controlled study, SleepSense demonstrates a promising recognition rate for breathing section, on-bed movement, and bed exit detection. Our 75-minute sleep study demonstrates the wide usability of SleepSense. The contribution of our work is summarized as follows:

- Developed a noncontact sleep monitoring system using a COTS-based Doppler radar sensor, which can capture the movement and breathing signal precisely. We validated the captured movement signal using the ground truth signal provided by the accelerometer and the breathing signal using the ground truth signal provided by the airflow sensor;
- Designed a new sleep status recognition framework. In this framework, it performs the signal segmentation, time-domain and frequent-domain features extraction, and sleep status detection, including on-bed movement, bed exit, and breathing section.
- Performed a short-term controlled study and a 75-minute sleep study to evaluate the performance and usability of SleepSense. In the short-term controlled study, SleepSense was able to distinguish the recall rate for breathing section, on-bed movement, and bed exit detection, which is 99.3%, 86.1%, and 70.0%, respectively. In the 75-minute sleep study, we also performed the sleep status classification, then compared the extracted breathing rate via SleepSense with the ground truth signal provided by the airflow sensor. The error rate was only 6.65%.

The remaining sections of this paper are organized as follows: Section II discusses the design considerations and challenges for SleepSense. Section III elaborates the COTS-based Doppler radar sensor system design. In Section IV, we propose a sleep status recognition framework to locate the on-bed movement, bed exit, and breathing section. Furthermore, a novel peak detection algorithm is proposed to calculate the breathing rate. In Section V, we perform two sets of experiments to evaluate the SleepSense in the short-term and 75-minute sleep study. Section VI discusses interesting findings and system limitations. Finally, Section VII concludes the paper and describes future work.

[1]We emphasize "sleep status" to differentiate the "sleep stage" defined in the clinics.

II. Design Considerations

A. Design Challenges

There are more than 12 million people suffering from obstructive sleep apnea and about 40 million people with insomnia and chronic sleep disorders in U.S. [28]. Technologies offer a number of sleep monitoring systems for sleep disorder diagnostics and treatment. We address the challenges for sleep monitoring system design.

1) Unobtrusiveness: The sleep monitoring system should be unobtrusive because the subjects feel nervous or uncomfortable when they are monitored physically. In the obstructive sleep monitoring methods, such as PSG and actigraphy, the user has to wear the sensors or the sensors have to be attached. Consequently, the uncomfortable feeling of wearing these sensors or devices may cause the subject to have difficulty either falling asleep or maintaining sleep.

2) Privacy: The sleep monitoring system should protect the patient's privacy. The patient privacy should be strictly protected because it gains increasingly significance recently, especially when it comes to the sleep, an extremely personal topic. Recording raw video and audio signal raise patient concerns about privacy.

3) Cost-Effective Implementation: The sleep monitoring system should be cost-effective. An affordable sleep monitoring method can reach more people and help them perform sleep quality assessments and potentially identify disorders at the earliest stage, thereby reducing a patient's financial burden in the long term.

To address the aforementioned challenges, the proposed sleep monitoring system employs a Doppler radar sensor to capture the sleep status in a noncontact way. Our method also performs all the sleep-related data processes in a local embedded computer. Other unrelated sleep information will be screened and removed before uploading to a server. Therefore, the implemented sleep monitoring system can truly protect individual privacy. Furthermore, the implementation is cost-effective because the Doppler radar sensor is built on several COTS-based components.

B. Sleep Status of Interest

Sleep, a combination of physiologic and behavioral processes, is a period of inactivity and rejuvenation [29]. During sleep, breathing patterns and movement patterns are of particular interest as they convey important information about a person's sleep state [30], [31] and are closely associated with sleep quality. On the basis of breathing patterns and movement patterns, we define three sleep statuses: on-bed movement

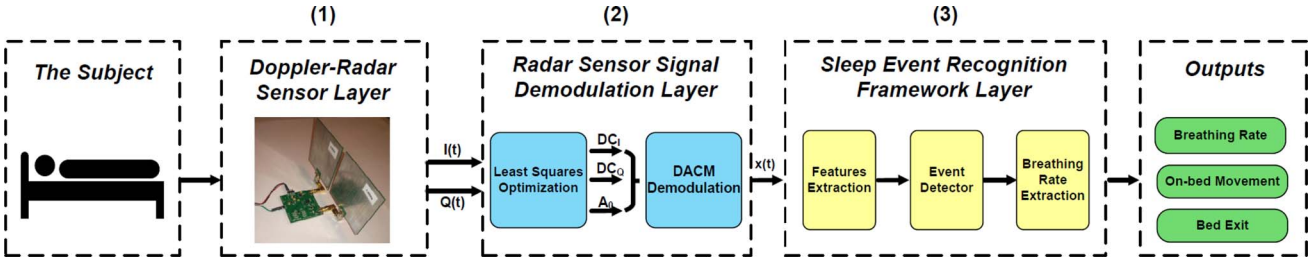

Fig. 1. The function block diagram of Sleepsense system. (1) Doppler radar sensor. (2) Radar signal demodulation. (3) Sleep status recognition framework.

event, bed exit event, and breathing section. We focus on event recognition when people are already in the sleep state. The on-bed movement event is a movement such as turn over or arm trembling. The breathing section is when a subject is still on the bed (no observable body movements). The bed exit event refers to the bed exit movement that indicates interruption of the sleeping state. Successful recognition of these three sleep status states is the basis for obtaining breathing and movement distribution patterns.

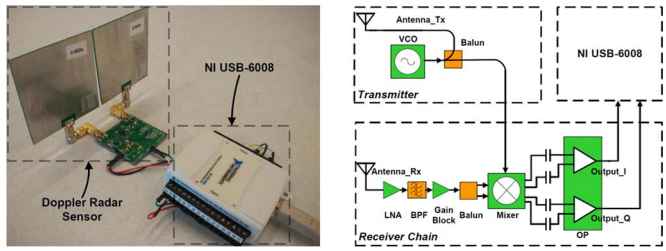

(a) (b)

Fig. 2. The Doppler radar sensor and its function block diagram. (a) The Doppler radar sensor and NI-USB 6008 data acquisition device. (b) The function block diagram of Doppler radar sensor.

III. COTS-Based Doppler Radar Sensor System Design

A. System Overview

SleepSense is a noncontact and cost-effective sleep monitoring system that continuously detects the sleep-related status and obtains the breathing rate. Fig. 1 shows the overall system architecture of SleepSense. First, the Doppler radar sensor captures the sleep-related signal from the subject and outputs the baseband signal I/Q. Then, the demodulation layer employs an extended DACM demodulation algorithm to obtain the displacement signal $x(t)$. The sleep status recognition framework, finally, extracts the sleep status-related features from the displacement signal $x(t)$ and classifies the sleep status. In the meantime, a novel breathing rate extraction algorithm calculates the respiration rate. Specifically, three layers are introduced here:

1) Radar Sensor Hardware Layer: The Doppler radar sensor can be used for human motion detection. Specifically, the radar sensor generates a single-tone carrier signal which is transmitted to the subject. Once the microwave reaches the position of subject, the chest wall or body displacement will be modulated into the phase shift in the microwave reflection. The phase shift includes both movement and respiration information. This phase shift is proportional to the corresponding movement displacement. By demodulating this phase information properly, we can obtain the movement displacement signal.

2) Radar Signal Demodulation Layer: The radar signal demodulation layer handles the baseband radar I/Q signal, which contains the target displacement information. In order to acquire the displacement information, we employ an extended DACM algorithm to demodulate the baseband signal. Then, the displacement signal $x(t)$ is transmitted to the sleep status recognition framework for further processing.

3) Sleep Status Recognition Framework Layer: The sleep status recognition framework performs further signal processing on the displacement signal $x(t)$. Specifically, the sleep status recognition layer frames the $x(t)$ into short segments and extracts the multiple time and frequency-domain features for each segment. Then, based on these features, the status detector categorizes these segments into three classifications: breathing section, on-bed movement, or bed exit. The status detector is a decision-tree based classifier. Based on the classification result, this layer also uses a breathing rate extracting algorithm to calculate the breathing rate when the subject has no gross body movements.

B. Doppler Radar Sensor Hardware Design

The purpose of our proposed system is to perform sleep monitoring in a remote and cost-effective manner. This aim is achieved by using a Doppler radar sensor. For several decades, Doppler radar sensors have detected human vital signs, such as respiration and heartbeat. Studies [32]–[34] have reported progress in sensing vital signs. Doppler radar-based biomotion sensors are used for sleep monitoring [35] and sleep/wake measurement [36]. There are also commercial sleep monitoring products [37], [38] based on Doppler radar from Resmed, in which they adopt the linear demodulation. In our case, we design and build this sensor based on the COTS components, which can also sense human motions. Fig. 2 shows the hardware system and its function block diagram. The Doppler radar sensor adopts direct-conversion radar architecture to capture the subject movement and breathing signal. In the circuit implementation, as shown in Fig. 2(b), the VCO in the transmitter generates a carrier signal at 2.4 GHz. The VCO also provides local oscillate (LO) to the mixer in the receiver chain. The output power of this transmitter is less than 0.01 dBm. A low noise amplifier (LNA), a band pass filter (BPF), a gain block, a

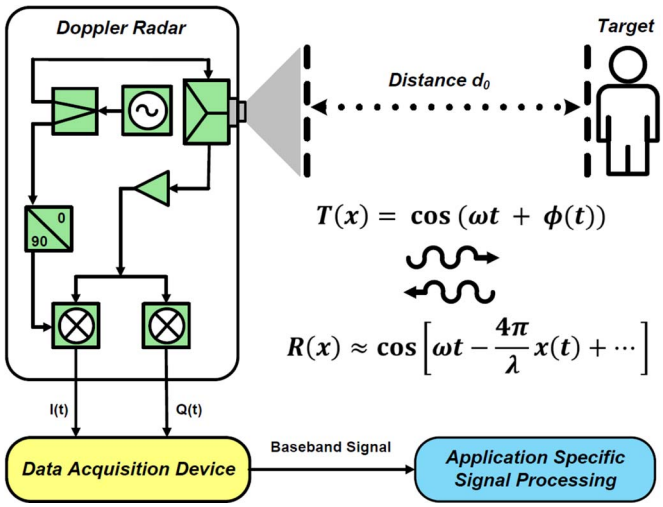

Fig. 3. The principle of Doppler radar sensor for human motion detection.

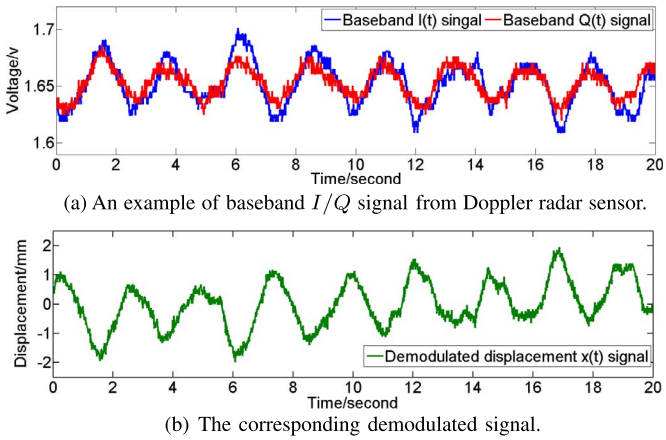

(a) An example of baseband I/Q signal from Doppler radar sensor.

(b) The corresponding demodulated signal.

Fig. 4. (a) Baseband radar I/Q signal. (b) Corresponding demodulated signal $x(t)$.

balun, a mixer and two baseband operational amplifiers (OPs) form the receiver chain. The LNA amplifies the received signal at 2.4 GHz. The interferences with frequencies outside the 2.4 GHz band is removed by the BPF. A gain block is adopted to further amplify the received signal. Two OPs with the same gain of 40 dB are used to amplify the down-converted $I(t)$ and $Q(t)$ baseband signals [39]. Lastly, for simplicity, we employ an NI Data Acquisition device (DAQ), NI USB-6008, to digitize the baseband $I(t)$ and $Q(t)$ signals. This NI DAQ device can be replaced by any other DAQ devices or self-customized DAQ device to reduce the implementation cost.

C. Radar Sensor Signal Demodulation

The baseband signal demodulation requires an understanding of Doppler radar theory. Fig. 3 briefly illustrates basic Doppler theory. The Doppler radar sensor transmits the continuous-wave signal $T(t)$

$$T(t) = A_T \cos\left(\omega t + \phi(t)\right). \tag{1}$$

Then, the transmission wave is received as $R(t)$

$$R(t) = A_R \cos\left[\omega t - \frac{4\pi d_0}{\lambda} - \frac{4\pi x(t)}{\lambda} + \phi\left(t - \frac{2d_0}{c}\right)\right] \tag{2}$$

where A is the amplitude. ω represents the angular velocity. $\phi(t)$ is the time-varying phase. λ is the wavelength. c is the speed of light. d_0 is distance between the Doppler radar and the subject. $x(t)$ denotes the time-varying displacement caused by sleep related status.

The $R(t)$ then generates two baseband signals including $I(t)$ and $Q(t)$. $I(t)$ is the in-phase signal

$$I(t) = A_I \cos\left[\frac{4\pi x(t)}{\lambda} + \frac{4\pi d_0}{\lambda} - \phi\left(t - \frac{2d_0}{c}\right)\right] + \mathrm{DC}_I \tag{3}$$

$Q(t)$ is the quadrature signal

$$Q(t) = A_Q \sin\left[\frac{4\pi x(t)}{\lambda} + \frac{4\pi d_0}{\lambda} - \phi\left(t - \frac{2d_0}{c}\right) + \phi_0\right] + \mathrm{DC}_Q \tag{4}$$

where A_I is the amplitude of the in-phase signal. A_Q is the amplitude of the quadrature signal. ϕ_0 is the phase offset between $I(t)$ and $Q(t)$. DC_I and DC_Q are the DC offsets in I/Q channels, respectively.

The NI USB-6008 samples the baseband radar signals, $I(t)$ and $Q(t)$, at 100 Hz. An example of acquired baseband radar I/Q signals for several breathing sections is shown in Fig. 4(a).

In our work, for simplicity, we neglect the constant phase offset, $4\pi d_0/\lambda + \phi(t - 2d_0/c)$, in (3) and (4). Assuming that the gain imbalance is 1 (the ratio of A_I and A_Q is 1), and phase imbalance (ϕ_0) is 0. Therefore, (3) and (4) can be described as

$$\begin{cases} I(t) = A_0 \cos\left(\frac{4\pi x(t)}{\lambda}\right) + \mathrm{DC}_I \\ Q(t) = A_0 \sin\left(\frac{4\pi x(t)}{\lambda}\right) + \mathrm{DC}_Q. \end{cases} \tag{5}$$

According to trigonometric identities, (5) can be transformed into

$$\left(\frac{I(t) - \mathrm{DC}_I}{A_0}\right)^2 + \left(\frac{Q(t) - \mathrm{DC}_Q}{A_0}\right)^2 = 1. \tag{6}$$

Therefore, the samples of I/Q channels stay on a circle whose center is $(\mathrm{DC}_I, \mathrm{DC}_Q)$ with a radius of A_0.

The least squares optimizations [34], then, is employed to obtain the circle and identify the three unknown parameters: DC_I, DC_Q, and A_0.

After identifying the DC component offsets, the arctangent demodulation method can derive the displacement signal $x(t)$ by solving the arctangent function in (7)

$$x(t) = \arctan\left(\frac{Q(t) - \mathrm{DC}_Q}{I(t) - \mathrm{DC}_I}\right) \times \frac{4\pi}{\lambda}. \tag{7}$$

However, the arctangent demodulation method suffers from the phase discontinuity issue or phase wrapping issue when the movement is in large scale motion

$$\omega(t) = \frac{\mathrm{d}}{\mathrm{d}t}\left(\arctan\frac{Q(t)}{I(t)}\right). \tag{8}$$

Specifically, when the demodulation exceeds the native codomain range $((-\pi)/2, \pi/2)$ of the arctangent function, a discontinuity problem will occur and the demodulation results will be inaccurate. The original DACM algorithm in (8) could be applied to avoid such a discontinuity problem. It is a derivative to the arctangent function and could be written as (8). The calculation of $w(t)$, however, is very sensitive to noise in the traditional DACM algorithm. Thus, in this paper, an extended DACM algorithm proposed by Wang *et al.* [40] is adopted. Here, $\Phi(t)$ is defined as

$$\Phi(t) = \frac{4\pi x(t)}{\lambda} + \frac{4\pi d_0}{\lambda} + \phi\left(t - \frac{2d_0}{c}\right) \tag{9}$$

which is the part inside cosine function in (3). Since the phase offset $4\pi d_0/\lambda + \phi(t - 2d_0/c)$ is constant, once $\Phi(t)$ is obtained, $x(t)$ can be directly retrieved. In the digital domain, the procedure of differentiation is usually approximated by forward difference, so the extended DACM algorithm can be formulated in a discrete form, as shown in (10), which adds an integration procedure to retrieve the phase information and suppress the noise caused by the differentiator in the meantime

$$\Phi[n] = \sum_{k=2}^{n} \frac{I[k]\{Q[k] - Q[k-1]\} - \{I[k] - I[k-1]\}Q[k]}{I[k]^2 + Q[k]^2}. \tag{10}$$

Fig. 4(b) shows a demodulated signal using this extended DACM algorithm.

IV. Sleep Status Recognition Framework

In this section, we present the sleep status recognition framework, which performs the signal segmentation, time-domain and frequent-domain features extraction, and sleep status detection, including on-bed movement, bed exit, and breathing section.

A. Framework Structure

The architecture of this framework comprises signal segmentation, features extraction, sleep status recognition, and a breathing rate extraction algorithm, as shown in Fig. 5. First, the displacement signal $x(t)$ is framed into short segments with the window length of 512 samples, corresponding to 5.12 seconds with a sampling rate of 100 Hz. This segmentation setup is empirically chosen according to the observation in the study. In addition, it well associates the segment with body movement in one period and benefits further processing. Then, the framework extracts the features for each segment and classifies these segments into three sleep status: on-bed movement event, bed-exit event, or breathing section. Simultaneously, breathing rate is obtained by using the novel breathing rate extraction algorithm.

B. Features Extraction

The sleep status is characterized with time-domain and frequency-domain features. For instance, the breathing section has a subtle fluctuation in the displacement signal $x(t)$ in terms of amplitude and frequency, while the on-bed movement event and bed exit event have relatively larger changes. To represent these three different sleep statuses, we, therefore, extract five features including two statistical features, two frequency-domain features, and a non-linear time-series feature, i.e., root mean square (RMS), mean crossing rate (MCR), energy, mel-frequency cepstral coefficients-based coefficients (MFCC-based coefficients), and sample entropy, which are shown in Table I. Note that the values for the aforementioned features are obtained from each 512 samples of non-overlapping windows.

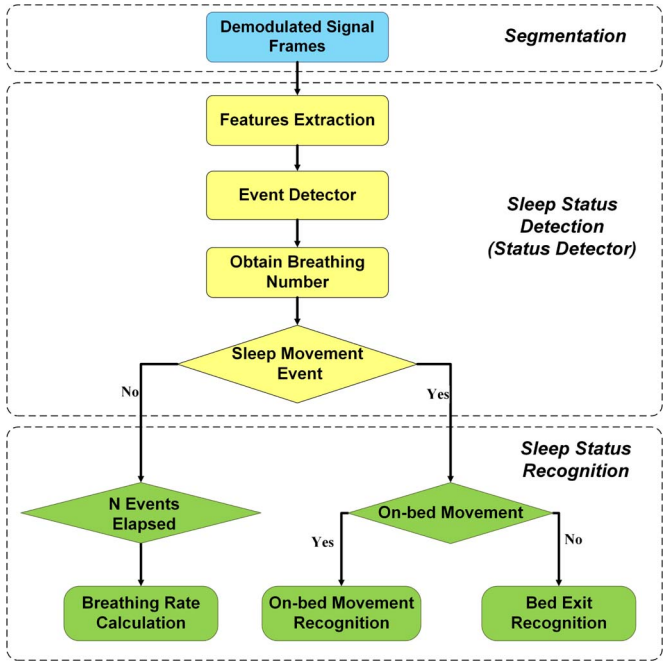

Fig. 5. The flow chart of sleep status recognition framework, consisting of segmentation, sleep status detection, and sleep status recognition.

RMS is a parameter that implies the size of signal amplitude, namely, the strength of the subject's movement in our case, which is defined in (11)

$$\text{RMS} = \sum_{i=0}^{N_s} \sqrt{\frac{A(i)^2}{N_s}} \tag{11}$$

where $A(i)$ is the amplitude of the demodulated signal $x(t)$. N_s is the sample number. Consequently, if the amplitude of $x(t)$ has large variability, the RMS value varies correspondingly, indicating an existence of dramatic sleep movement.

MCR is defined as the rate when the demodulated signal $x(t)$ passes across the mean value over the total samples. To be specific, it counts the occurrence times (OT) of $x(t)$ that go above or below the mean value, as defined in (12)

$$\text{OT} = \sum_{k=1}^{N_s - 1} \mathbf{1}_A\left((x_k - \bar{x})(x_{k+1} - \bar{x}) < 0\right) \tag{12}$$

where $\bar{x}$ is the mean value of total N_s samples, and $\mathbf{1}_A(\cdot)$ is the indicator function. Then, the MCR can be calculated by using (13)

$$\text{MCR} = \frac{1}{N_s - 1} \sum_{k=1}^{N_s - 1} \mathbf{1}_A\left((x_k - \bar{x})(x_{k+1} - \bar{x}) < 0\right). \tag{13}$$

TABLE I
THE LIST OF SELECTED FEATURES

No.	Feature List	Feature Definition
1	Root Mean Square (RMS)	The quadratic mean value of the signal
2	Mean Crossing Rate (MCR)	Number of changes between below mean & above mean
3	Energy	The energy over the window
4	MFCC-based Coefficients	The cepstral coefficients obtained following the procedure in Fig. 6, without going through a Mel-filter
5	Sample Entropy	The regularity and complexity of the distribution of the signal

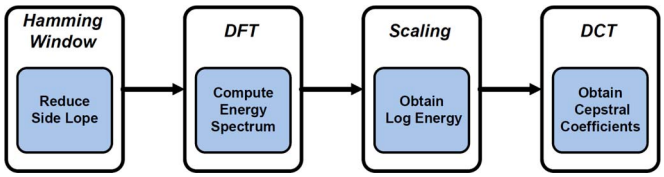

Fig. 6. The procedures for the MFCC-based feature extraction, which are Hamming filtering, DFT, scaling, and DCT.

In our case, the on-bed movement and bed exit movement will produce dramatic fluctuation in terms of frequency. Therefore, the MCR values are various for these three sleep statuses.

Energy is a common frequency domain feature in the signal process. We also extract the energy distribution of each segment. A segment of the demodulated signal has 512 samples, forming the sequence

$$x_1, x_2, \ldots, x_n, \ldots, x_{N_s} \tag{14}$$

where $N_s = 512$. Then, the energy can be acquired by taking the finite Fourier transforms of this sequence as defined in (15)

$$E = \sum_{n=0}^{N_s-1} \left| x(n) e^{-j2\pi kn/N_s} \right|^2. \tag{15}$$

Obviously, the status of movements, such as bed exit movement and on-bed movement, has larger energy than the breathing section.

Another commonly used frequency-domain feature for analysis is MFCC, especially in the audio signal processing area. The study [41], [42] has proved that MFCC features are effective to represent the Doppler signatures and employs the MFCC coefficients to recognize various human activities. Likewise, we also compute MFCC features for each segment. Fig. 6 illustrates steps to extract the MFCC-based coefficients. It employs a Hamming window to process the segmented displacement signal $x(n)$

$$\widetilde{x}(n) = x(n) \times W(n) \tag{16}$$

where $x(n)$ is the displacement signal. $W(n)$ is the n sample long Hamming window. Followed by performing the discrete Fourier transform (DFT), as shown in (17), which is applied to each frame to obtain the energy distribution in the frequency-domain

$$X(k) = \sum_{n=0}^{N-1} \widetilde{x}(n) \exp\left(\frac{-j2\pi k}{N}\right), 0 \le k \le N-1 \tag{17}$$

where $\widetilde{x}(n)$ is the displacement signal after the Hamming window and n denote number of samples. N is the length of DFT. However, unlike the traditional MFCC technology which uses a Mel-filter banks to block a certain frequency range in the audio signal, in our case, we do not implement the Mel-filter banks because the frequency features of on-bed movement, bed exit, and breathing section are all in the frequency domain. Therefore, we must keep all the frequency features in all frequency domains, and no filter is needed. We then scale the data with log function, as shown in (18), in each frame to get the log energies

$$s(k) = \ln\left(|X_i(k)|^2\right), 0 \le k \le N-1. \tag{18}$$

We employ (19) to perform discrete cosine transform (DCT) to obtain the corresponding cepstral coefficients of each frame

$$C(m) = w(m) \sum_{k=0}^{k=N} s(k) \cos\frac{\pi(2k-1)(m-1)}{2N}, 1 \le m \le N \tag{19}$$

where $w(m)$ is

$$w(m) = \begin{cases} \frac{1}{\sqrt{N}} & m = 1 \\ \sqrt{\frac{2}{N}} & 2 \le m \le N. \end{cases}$$

Finally, we extract the sample entropy for each frame because the sample entropy provides an enhanced method to measure the complexity and regularity of the signal, which can be derived by (20)

$$\text{SampleEn}(m, r, N) = -\ln\left(\frac{\phi'^m(r)}{\phi'^{m+1}(r)}\right) \tag{20}$$

where

$$\phi'^m(r) = (N-m+1)^{-1} \sum_{i=1}^{N-m+1} C_i'^m(r). \tag{21}$$

The m is the embedding dimension. r is the tolerance. The number of data points is N. In our case, the displacement signal from the breathing section has more regularity and less complexity than the displacement signal from the on-bed movement and bed exit status, thus having the distinguished sample entropy value.

C. Breathing Rate Estimation

In this section, we present the breathing rate calculation algorithm using an adaptive-threshold based peak detection method. Because the demodulated breathing displacement signal is similar to the trigonometric signal, as shown in Fig. 10. A pair of peak and valley corresponds to a breathing section. Therefore, the extraction of the breathing rate is to count the number of pairs of peaks and valleys in the displacement signal. Traditionally, this aim can be achieved by employing a general peak detection method with the fixed threshold. The

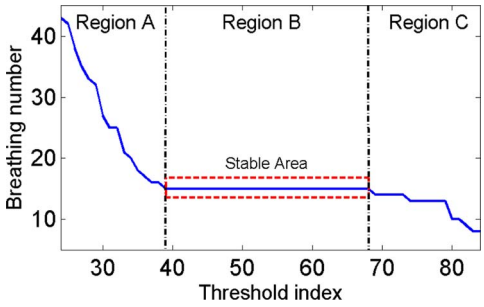

Fig. 7. A peak detection with adaptive threshold example. In region *A* and region *C*, the breathing number is not consistent, implying sensitivity to random noise. However, the breathing number that corresponds with the most flat area, Region *B*, is desired.

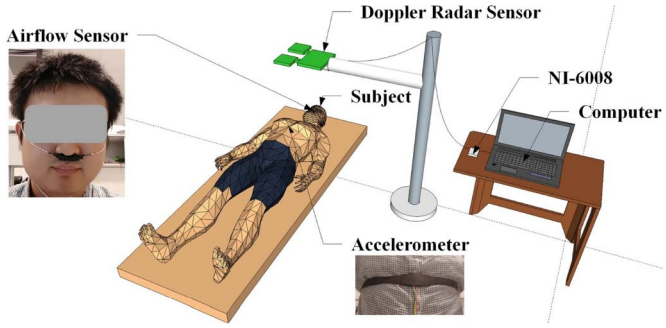

Fig. 8. The experimental setup: the subject lies his back on a mattress, and the radar locates on the top of chest of the subject with the distance of 1 meter. Meanwhile, an airflow sensor and an accelerometer sensor are attached to serve as the ground truth signal.

threshold is defined as the value difference between the peak (or valley) and its neighboring values. However, during sleep the breathing signals from different subjects usually vary in magnitude and frequency, even the same subject has various breathing patterns. Using the traditional threshold-fixed method will result in inaccurate peak detection, leading to a poor breathing rate calculation. Other methods based on Fourier transform [43], [44] can be employed to perform the breathing rate calculation. Our method is robust in suppressing noise and easy to implement without complex calculations for portable applications. Therefore, we utilize a peak detection algorithm with an adaptive threshold to resolve this issue.

When a segment of displacement signal $x(n)$ arrives, the proposed breathing rate extraction algorithm obtains the relationship between the breathing number and the threshold value. Specifically, the algorithm goes through all the threshold values from 0 to the maximal magnitude difference. For each threshold value, the corresponding number of peaks (or valleys) is detected, we depict this relationship in Fig. 7. The threshold index in x-axis represents the different threshold values that are used for peak detection. The breathing number in y-axis is the detected breathing number that corresponds with a certain threshold value. In Region *A* and Region *C*, the breathing number varies largely for these threshold indexes. It means that the detected breathing number experiences a large variability when the threshold value changes with a small value, representing the sensitivity to random noise and false peak detections. However, in the most flat Region *B*, the breathing number stay unchanged when the threshold increases, which implies that most of the random noise is ignored and only the true peaks are countered. Therefore, the breathing number that corresponds with the most flat area is obtained. The breathing rate extraction algorithm is explained in detail in *Algorithm 1*.

Algorithm 1 Peak detection algorithm with adaptive threshold

Input: Demodulated signal $x(t)$
Output: Numbers of detected breaths

Obtain the max and min of input signals
$delta = \max - \min$
$lookForMax =$ true
for $thresh = 0$ to $delta$ **do**
  for all points of input signal **do**
    if $dataValue < currentMin$ **then**
      Update $currentMin$
    if $dataValue > currentMax$ **then**
      Update $currentMax$
    if $lookForMax == true$ and $dataValue < (currentMax - thresh)$ **then**
      Record the peak
      Update $currentMax$
      $lookForMax = false$
    if $lookForMax == false$ and $dataValue > (currentMin + thresh)$ **then**
      Record the valley
      Update $currentMin$
      $lookForMax = true$
Find the most flat region and obtain the breathing numbers

V. Experiments and Results

In this section, we conduct several experiments to evaluate SleepSense. First, the experiment setup is presented, followed by verification of the sampled signal from SleepSense using the ground truth signal from the accelerometer sensor and airflow sensor. Then, we perform a short-term study for qualitatively evaluation of the performance of SleepSense. Finally, we perform a 75-minute sleep study, which focus on the real-case usability evaluation.

A. Experimental Setup

The experimental setup is illustrated in Fig. 8. The Doppler radar sensor is located on the top of the subject with a distance of one meter. An NI DAQ device (NI USB-6008) samples the baseband signal at 100 Hz, in the meantime, it synchronizes the radar signal and the reference signal. Simultaneously, an airflow sensor and an accelerometer provide the ground truth for the breathing and movement signal. Weka 3 [45] is used to implement the decision-tree based classifier, in which the thresholds for each feature are determined by Weka 3 adaptively.

B. Breathing and Movement Signal Verification

The aim of this section is to verify the sampled sleep status signal from SleepSense. In order to accomplish this goal, we

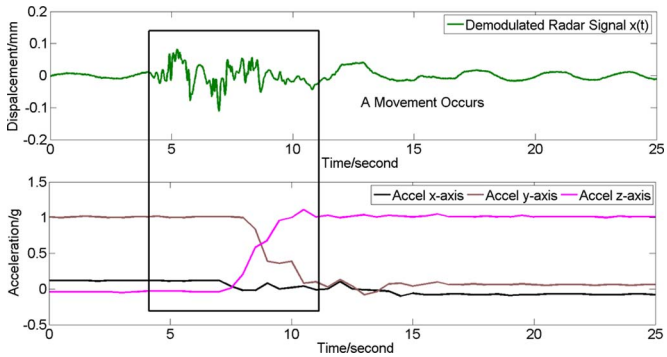

Fig. 9. When a movement occurs, there is a large-magnitude and fast-frequency fluctuation in the demodulated signal. The x-axis, or y-axis, or z-axis value of the accelerometer changes correspondingly.

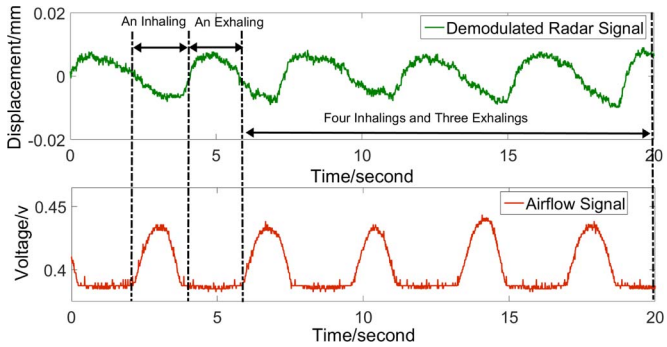

Fig. 10. The top sub-picture is the breathing signal from the SleepSense system; the bottom sub-picture is the ground truth provided by the airflow sensor. They are matched.

employ an accelerometer and an airflow sensor to serve as the ground truth signal. Specifically, the accelerometer, which is attached to the subject's chest as shown in Fig. 8, can detect subject movement accurately because its X-axis, Y-axis, and Z-axis values experience changing levels when a movement occurs. The airflow sensor, which is attached in the nostril area as shown in Fig. 8, captures the breathing signal because it is a thermistor-based airflow sensor and the temperature around the nostril area changes when the subject inhales and exhales.

First, we aim to validate the sampled movement signal. Fig. 9 demonstrates the relationship between the demodulated signal from SleepSense and the signal from the accelerometer sensor. We notice that there is a large-magnitude and fast-frequency fluctuation in the demodulated signal, which indicates a movement. Correspondingly, it has obvious value changes in three axes of the accelerometer. Therefore, it has been proven that the sampled movement signal is the actual movement signal.

Then, we verify the acquired breathing signal from SleepSense via an airflow sensor. Fig. 10 illustrates the relationship between the breathing signal and ground truth signal. The demodulated radar signal are matched with the reference signal, which stems from the airflow sensor. A breathing section consists of an inhalation, a valley in the demodulated signal, and an exhalation, a peak in the demodulated signal. One breathing section corresponds with a peak in the reference signal, as shown in Fig. 10. Therefore, the breathing signal from SleepSense can be validated by the ground truth signal.

TABLE II
CONFUSION MATRIX OF SHORT TERM STUDY

Actual \ Predicted	On-bed movement	Bed exit	Breathing section	**Recall**
On-bed movement	93	10	5	86.1%
Bed exit	9	21	0	70.0%
Breathing section	3	0	405	99.3%
Precision	88.6%	67.7%	98.8%	

C. System Performance Evaluation

We perform the short-term controlled study to qualitatively examine the performance of the SleepSense system. Specifically, the sleep status recognition framework is evaluated, followed by the evaluation on the breathing rate extraction algorithm.

1) Data Collection: The data collection in this section follows the experimental configuration in Section V-A. Three subjects participated in the short-term controlled study. Their ages were 25 to 28 years, height 180 to 185 cm, weight 80 kg to 100 kg. Each subject performed four sets of on-bed movement tests and 10 sets of bed-exit tests. In each on-bed movement test, the subject laid on his back and remained still on the mattress. After 25 seconds, the subject turned over and remained still for the next 25 seconds. Finally, the subject changed back to lie on his back on the mattress. Each subject repeated the aforementioned steps three times in one test, which took roughly 3 to 4 minutes. In total, we acquired 12 groups of on-bed movement and 40 groups of bed exit.

2) Sleep Event Detection Accuracy: The SleepSense system processes the acquired data from the aforementioned sets of tests with the framework in Section IV. The classification results are based on the each epoch of 5.12 seconds, and the ground truth signals are from the accelerometer and air flows. The status detection confusion table is shown in Table II, where the left column represents the actual activities and the top row represents the predicted activities. We define the overall accuracy (ACC) to be the probability that all the events are recognized correctly, as shown in (22)

$$\mathrm{ACC} = \frac{\mathrm{TP} + \mathrm{TN}}{\mathrm{P} + \mathrm{N}} \tag{22}$$

where TP is true positive, TN is true negative, P is positive, and N is negative. The results show that the overall accuracy is 95.1%. In the case of on-bed movement recognition, the SleepSense system successfully distinguishes 93 segments from the total 108 segments labeled with on-bed movement. In terms of bed exit recognition, it recognizes 21 segments from the total 30 segments labeled bed exit. In the case of breathing section detection, SleepSense identifies 405 segments from the total 408 segments, which shows a high probability of correct recognition of the breathing section. No breathing section is recognized as the bed exit. It is the same for bed-exit recognition. This is because the features from the bed exit and breathing section vary dramatically in terms of time domain or frequency domain. However, the classification result for bed exit and on-bed movement events is inferior because some of the on-bed movements and bed-exit movements share the same features such as frequency and amplitude in movements.

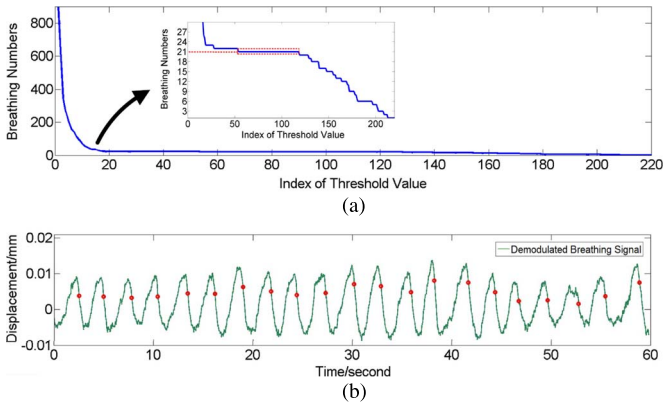

Fig. 11. The novel breathing rate extraction method using a novel peak detection algorithm with adaptive threshold. (a) Relationship between the detected breathing numbers and threshold values. (b) Detect peaks using a specific threshold value.

There are also some errors for on-bed movement and breathing section recognition, which is caused by the windowing issue. Specifically, because we employ the fixed length window in the segmentation, a movement may be incorrectly divided into several windows and lose the on-bed movement features, leading to misclassification. To improve the recognition of bed exit/entrance, we can consider other sensing modalities, such as adding another radar/infrared sensor to detect occupancy [46].

3) Breathing Rate Extraction: We verify the proposed breathing rate extraction algorithm by employing it on a short breathing signal, which is described in Fig. 11(b). The short breathing signal holds 60 s long, which is an excerpt from a normal breathing signal longer than 60 s. From the demodulated signal, we can observe that the breathing number is 21 during the 60 seconds. By applying the peak detection algorithm with adaptive threshold, we can obtain the relationship between breathing numbers and threshold index as shown in the top of Fig. 11(a). According to the algorithm, we look for the most flat region on the signal, which is zoomed in the upper part. The most flat region is circled by the red rectangle and the corresponding breathing number is 21. The breathing rate algorithm employs different threshold values to calculate the number of peaks. Therefore, this algorithm can detect different values of peaks based on different threshold values. The red dots, as shown in the bottom of Fig. 11(b), are a group of detected peaks based on specific threshold values. Note that, the red dots are not located at the top of breathing peaks, this is because we use different thresholds (the threshold typically goes from 0 to the maximal magnitude with a proper step) to detect the peaks. In some cases when using certain thresholds, the detected peaks are not located at the top of the waveform, but the number of detected peaks is right. In our algorithm, we obtain the relationship between threshold and detected peaks to determine the correct peak number.

D. A 75-Minute Sleep Monitoring Case Study

We also perform a 75-minute sleep monitoring study, which evaluates the wide usability of SleepSense in a real-case study.

The data are collected during a nap of one subject. Similarly, we deploy an airflow sensor and acceleration sensor on the subject to establish the ground truth for breathing and movement signal. The displacement signal is shown in Fig. 12(a). The sleep status recognition framework frames the 75-minute signal into small segments. The ground truth in Fig. 12(b) shows that it has a total of 4 on-bed movements and one bed exit. Others are the breathing sections. Because the duration of the on-bed movement exceeds the frame length, which is 5.12 seconds, two consecutive frames thus, contain one movement signal. Therefore, there are total 8 frames that represent the on-bed movement event. The total number of sleep status frames is 878. Only one frame is the bed-exit event, and the rest of the 869 frames are breathing sections. Finally, the trained sleep status detector in Section V-C processes all of these frames. These segments will be classified into three sleep statuses: on-bed movement, bed exit, or breathing section.

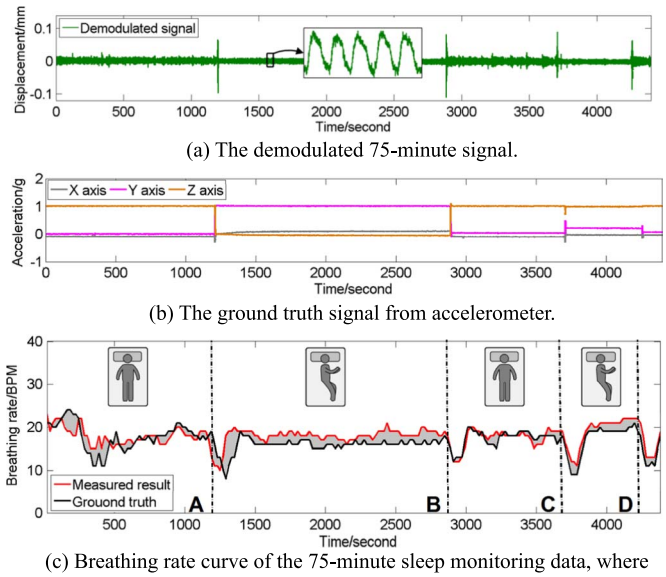

Fig. 12. (a) Demodulated signal (75 minutes) from the SleepSense system. (b) Ground truth provided by accelerometer. (c) Breathing rate for this 75-minute nap.

TABLE III
CONFUSION MATRIX OF THE 75-MINUTE SLEEP MONITORING STUDY

Actual \ Predicted	On-bed movement	Breathing section	**Recall**
On-bed movement	7	1	87.5%
Breathing section	0	869	100.0%
Precision	100.0%	99.9%	

The confusion matrix of the 75-minute sleep monitoring study is shown in Table III, where we focus on the evaluation of on-bed movement and breathing section detection where there is only one bed exit that is correctly recognized. In this test, SleepSense distinguishes all the breathing sections, which shows high accuracy. We note that the recognition rate for on-bed movement event detection is relatively lower because of the two misclassified on-bed movement statuses. The misclassification cases may be caused by the aforementioned windowing issue. The overall accuracy in this study is 99.9%, though the result is unbalanced because most of the segments are breathing sections.

Moreover, we calculate the breathing rate by averaging the breathing counts in the previous 20 windows, which is based on our trial and 20 gives the most accurate breathing rate. Fig. 12(c) demonstrates the overall breathing rate for this short period of sleep. Specifically, the red curve is the estimated result by using the SleepSense system. The black curve is the ground truth signal. These two curves are matched similarly. Both are about 18 BPM (Breath per Minute). We can observe that the breathing rate varies during sleep in Fig. 12(c). When the subject is going to fall asleep, the breathing rate is more irregular, which changes between 20 BPM and 10 BPM in region *A*. However, the breathing rate becomes stable when the subject falls asleep. At the end of sleep, the breathing rate experiences another level of change. An interesting phenomenon happens when the subject changes sleep position, which is associated with reduced breathing rates. This is because in the middle of the gross body movement, breathing activity is overwhelmed in body movement signals. Advanced signal processing will be considered to extract breathing signals in future work. In Fig. 12(a) of the 75-minute nap study, when gross body movements happen, the displacement signal shows instantaneous peaks in the time stamps of 1200, 2850, 3700, and 4250, which are totally different from the signal in breathing status as shown in the zoom in area of Fig. 12(a). This phenomenon indicates that the signal of breathing activities is overwhelmed by the signal of body movements. In this case, the breathing rate value during gross body movement is assigned with the last valid value of the breathing rate.

The mean of the breathing rate absolute error is 1.89 per minute, and the standard deviation is 1.47. The absolute error is defined as the absolute value of the difference between the measured result and the reference. Furthermore, we quantify the error rate (ER) between the SleepSense-measured result and the ground truth signal by using the area under the curve (AUC) method as shown in (23)

$$\mathrm{ER} = \frac{|\mathrm{AUC}(\mathrm{SleepSense}) - \mathrm{AUC}(\mathrm{GT})|}{\mathrm{AUC}(\mathrm{GT})} \tag{23}$$

where GT represents ground truth. We define the overall error rate as the ratio of the total area difference between the SleepSense-measured result and ground truth to the total ground truth area. The overall error rate is only 6.65%, which is the gray area in Fig. 12(c).

The error is caused by two factors: the on-bed movement and side sleep position. Fig. 12(c) shows a rising error rate (grey area) near the location where the subject changes to a different sleep position. This is because when an on-bed movement occurs, it is difficult for SleepSense to extract the breathing rate from that frame. However, the SleepSense will use the breathing number in the preceding frame that has no on-bed movement signal instead, causing the increased error rate. Another factor is the sleep position as seen from Fig. 12(c). The subject changes the sleep position from supine to side sleep and side sleep to supine four times during the nap. The error rate varies for different sleep positions. Specifically, the error rate is considerably lower when the subject is in the supine position. When the subject changes the sleep position to the side, the chest displacement is less significant, and the breathing signal becomes relatively weak for the subject who is in side sleep position. The performance of the breathing rate extraction algorithm diminishes correspondingly.

VI. Discussion

A. Parameters Selection

The experimental setup is based on our empirical observations in our preliminary set study. In our experimental test, a gross body movement takes approximately 5 s from the beginning to the end although we admit that this setup might be different according to the subject. Note that our framework is not tailored toward this setup and can be adjusted based on need. For example, it can be 6 s or 7 s setting if proper. In addition, for the simplicity of FFT transformation, we chose 512 samples in the study. As a result, we chose the segment length as 5.12 s. The aforementioned features are obtained from this 5.12 s segment. Note that 30 s is standard for sleep analysis where ground truth is obtained based on that, although this study did not use 30 s episode, this window length will be used in the future work when considering sleep stage analysis. In short-term controlled study, 25 s is only for emulating the still status between each body movement activities under the experimental protocols. The choice of 60 s episode of breathing signal is based on the work of Chazal *et al.* [47] that 60 s is proper for obstructive sleep apnea events detection. The episode length can also be conveniently changed to 30 s to follow the standard in sleep analysis.

B. Impact of Distance

In this section we discuss the impact of distance on the accuracy of the breathing rate extraction algorithm. The distance is defined as the length between the subject and antenna of Doppler radar sensor. Theoretically, the effective distance for our Doppler radar sensor is 1.5 meters based on its transmitter power. The power level of it is almost a thousand times less than the peak power of an ordinary global system for mobile communications (GSM) cellphone so it is safe for human-related applications. In our experiment, the distance is 1 meter. Based on our observation, the amplitude of the baseband radar I/Q signal is proportional to the distance between the subject and Doppler radar sensor. When the subject is far away from the Doppler radar sensor, the amplitude becomes diminished because it is difficult for the Doppler radar sensor to capture the chest wall displacement caused by breathing. The side sleep position experiences the same situation, which is discussed in the proceeding section. The downside of a smaller amplitude for the baseband radar signal is that it is more sensitive to interference from background noises, such as DC offsets and white noise caused by the Doppler radar sensor circuit. Therefore, we chose the distance of 1 meter as the suitable distance for our experiment.

In our study, we divide the sleep-related movement into two classifications: on-bed movement and bed exit. For the on-bed movement, we refer to it as the major on-bed movement,

whose amplitude is large, such as turn over. However, during sleep some micro on-bed movements such as arm trembling, leg jerk, and head movements occur. Because the Doppler radar sensor is located in the front of the subject's chest, it is difficult for the Doppler radar sensor to capture these leg jerk and head movements. Even though the radar can capture these signals, compared with these major on-bed movements, the time-domain and frequent-domain features of micro on-bed movement are not distinguished, which will be misclassified as the breathing section. However, these slight on-bed movements happen in the sleep [48], where rate of movement is lowest [31]. Therefore, micro-movement detection has limited impact on the performance of SleepSense.

C. Selected Features Discussion

Four scatter plots are shown in Fig. 13(a)–(d), respectively, to demonstrate the performance of the selected features, which are RMS, MCR, energy, MFCC-based coefficients, and sample entropy. Fig. 13(a) shows the feature of sample entropy versus mean of the first ten MFCC based coefficients. The samples of three status features located in three separate areas because MFCC-based coefficients discriminate the three statuses in the three ranges of y-axis values. Specifically, most breathing sections scatters in the range from -10 to 0 on the y axis. The bed exit and on-bed movement statuses, on the other hand, are located in the range from 10 to 20 and 0 to 10, respectively. Fig. 13(b) shows that the bed exit has the largest energy and breathing section has the least energy, because the frequency and displacement of the bed exit is much larger than that of breathing section and on-bed movement. Another feature RSM, which implies the signal amplitude, is much higher for bed exit than that of breathing section and on-bed movement, as shown in Fig. 13(c). In Fig. 13(d), because the demodulated signal in breathing section is a periodical signal, and it has the highest MCR among these three status. The bed exit movement, however, has the lowest MCR, because it is a one-time displacement.

D. Differences Between This and Related Work

Rahman *et al.* [49] use a Doppler radar to track sleep related variables including body movement and heart movement. By incorporating these variables, it can infer sleep versus wake classification and sleep stages classification. Compare to the work of Rahman *et al.*, our work focuses on activities classification including on-bed movement, bed-exit, and breathing. By extracting useful features, we have achieved higher recall rate and precision rate, as shown in Tables II and III, than those in the work of Rahman *et al.* Furthermore, we have elaborated the radar signal demodulation in our work which adopts a nonlinear demodulation. The nonlinear demodulation method enables more accurate respiration waveform extraction than the traditional linear demodulation. Our work is among the first studies reported with nonlinear demodulation. While in the work of Rahman *et al.*, the signal demodulation method is described briefly without details.

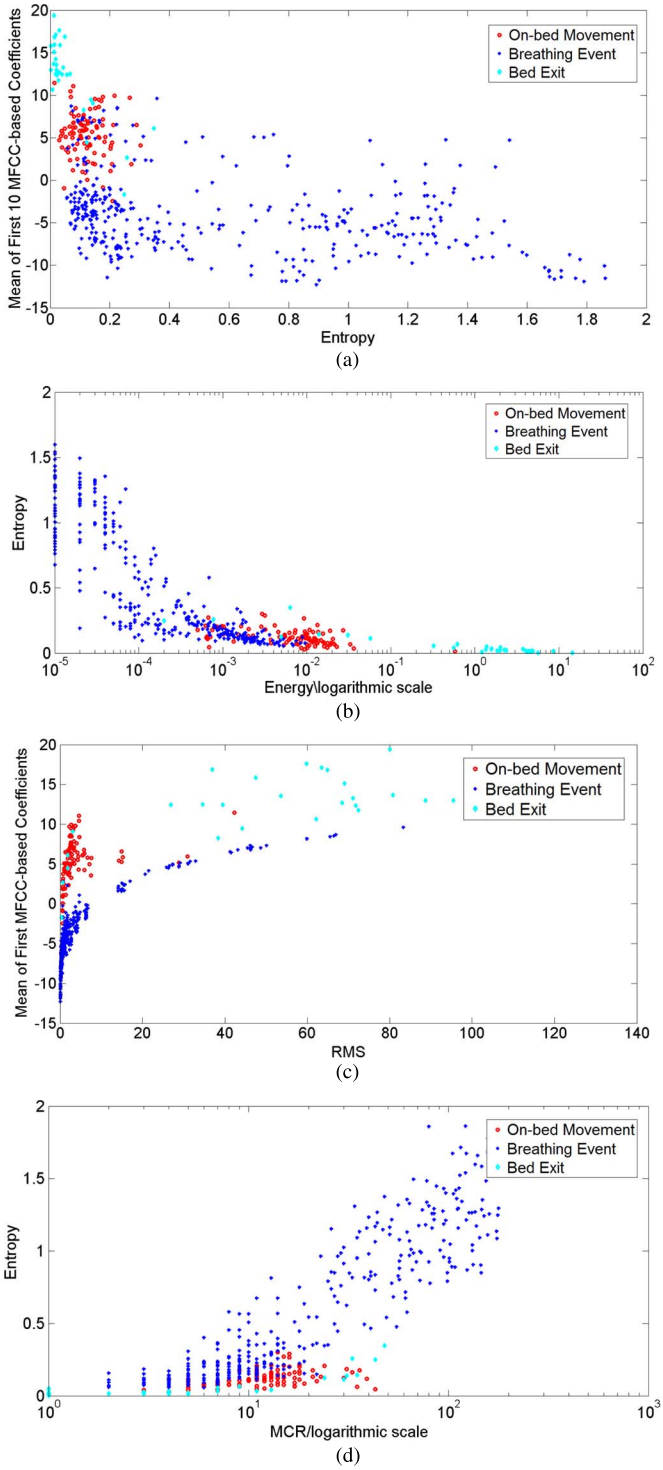

Fig. 13. The scatter plots for the entropy, MFCC-based coefficients, RMS, and MCR features distribution. (a) Entropy versus mean of first 10 MFCC-based coefficients. (b) Entropy versus energy. (c) RMS versus mean of first 10 MFCC-based coefficients. (d) Entropy versus MCR.

E. Body Movements During Sleep

In the short-term controlled study, we emulated the activities during sleep including turned over, remained still, and changed lying posture to show the feasibility and accuracy of our proposed system. The subject was awake in that study. However, the subject in the 75-minute nap study is actually in sleep, and the body movement is truly happened and in random pattern.

F. Incorporates With Other Non-Invasive Techniques

Though SleepSense is limited in its ability to detect micro on-bed movements, it can achieve higher performance by incorporating other non-invasive techniques such as actigraphy. Specifically, by placing an accelerometer sensor near the subject, we can obtain the location of micro on-bed movement which the SleepSense ordinarily cannot detect. These locations of micro on-bed movements are useful to recognize the deep sleep stage. Moreover, we can combine sub-sampled sound/vibrations with SleepSense to capture the sleep-related acoustic events. Similar to audio signals, sub-sampled sound/vibrations can still be captured with a cost-effective microphone, but sensitive audio information, such as speech, will not be included. Some recent studies, such as [17], [50], also share this similar insight. We can also combine a pressure-sensitive bed sheet [51], [52] to capture the sleep-related movement and posture events such as leg movement, body movement, and posture and body orientation. This movement and posture information are distributed in different sleep stages. By acquiring this information, we can perform the sleep stage classification precisely.

G. Capability of Sleep Stage Classification

In this study, we focus on monitoring sleep and extracting meaningful sleep information. The acquired the breathing pattern and movement distribution pattern are particularly useful to infer the different sleep stage [30], [31], even assess the sleep quality further [53]. The sleep research community generally divides the sleep into two categories: non-rapid eye movement (Non-REM) sleep stage and rapid eye movement (REM) sleep stage. The Non-REM sleep stage can be further classified into light sleep stage and deep sleep stage. The light sleep stage is transition from being awake to falling sleep, in which the body disengages from the surrounding and become relax for the arrival of deep sleep stage, thus results in frequent on-bed movements. When it comes to deep sleep stage, the body is totally relaxed for tissue repair and energy resort. Therefore, the frequency of on-bed movement is lowest and the breathing pattern is stable. In the REM Stage, where body is paralyzed because of the muscle immobility, only few on-bed movements occur occasionally. The breathing pattern, however, is irregular as the brain is active and dream occurs [54]. In summary, first, in terms of movement distribution, the rate of movement is lowest during deep sleep stage [31], REM sleep stage has fewer movements than light sleep stage because of the body paralysis [55], and light sleep stage is characterized with the frequent movements. Second, breathing patterns vary when it comes to the REM sleep stage since the REM stage is characterized with irregular breathing patterns [48], whereas the breathing patterns of Non-REM sleep stage are relatively stable. Therefore, our system is able to provide some information to perform the sleep classification, thus determine the sleep quality. Moreover, by incorporating our system with other non-invasive methods, SleepSense will be able to capture small body movements and provide fine-grained sleep quality assessments, which will be included in the future study.

VII. Conclusion and Future Work

In this paper, we present a non-contact and cost-effective sleep monitoring system, SleepSense, based on the Doppler radar sensor, which can discriminate various sleep status stages and extract the breathing rate accurately. In the implementation of SleepSense, we extract several time-domain and frequency-domain features and employ the decision-tree based classifier to recognize different sleep status, including breathing section, bed exit, and on-bed movement. The breathing rate, then, is calculated using a novel breathing rate extraction algorithm. We also empirically demonstrate the effectiveness of SleepSense in the short-term controlled study and the 75-minute real case study. The SleepSense can identify the on-bed movement, bed exit, breathing section, and extract the breathing rate with an acceptable accuracy rate and wide useability. We also perform the sleep stage classification based on the acquired information from SleepSense. By deploying the proposed sleep monitoring system at home, it can help people to assess sleep quality, even diagnose the sleep disorders at the earliest stages.

In the future, the system will be further enhanced in six aspects. First, the sleep onset detection will be included in the system. Second, the evaluation will include subject moving to sit up from lying down in bed to ensure this would not be falsely scored as bed exit. Third, we will comprehensively evaluate the overnight recording performance including the events detection accuracy and breathing rate accuracy with clinical instruments, such as PSG, adopted as the ground truth. Fourth, we will incorporate the other unobstructed monitoring methods to reduce the misclassification cases. Fifth, we will validate performance on recordings not used for development. Lastly, we will enhance the performance of SleepSense by implementing a radar demodulation method on the FPGA platforms, which is more efficient and can achieve the real-time demodulation for the baseband signal. Based on the acquired sleep pattern which includes breathing and movement distribution patterns, we will build SleepSense as a personalized sleep monitoring system.

References

[1] Y. Zhuang, C. Song, A. Wang, F. Lin, Y. Li, C. Gu, C. Li, and W. Xu, "Sleepsense: Non-invasive sleep event recognition using an electromagnetic probe," in *Proc. IEEE 12th Annu. Body Sensor Networks Conf.*, Boston, MA, Jun. 2015, pp. 1–6.

[2] R. D. Vorona, M. P. Winn, T. W. Babineau, B. P. Eng, H. R. Feldman, and J. C. Ware, "Overweight and obese patients in a primary care population report less sleep than patients with a normal body mass index," *Archives Intern. Med.*, vol. 165, no. 1, pp. 25–30, 2005.

[3] K. Spiegel, K. Knutson, R. Leproult, E. Tasali, and E. Van Cauter, "Sleep loss: A novel risk factor for insulin resistance and type 2 diabetes," *J. Appl. Phys.*, vol. 99, no. 5, pp. 2008–2019, 2005.

[4] D. Brooks, R. L. Horner, L. F. Kozar, C. L. Render-Teixeira, and E. A. Phillipson, "Obstructive sleep apnea as a cause of systemic hypertension. Evidence from a canine model," *J. Clin. Invest.*, vol. 99, no. 1, pp. 106, 1997.

[5] M. S. Aloia, J. Arnedt, J. D. Davis, R. L. Riggs, and D. Byrd, "Neuropsychological sequelae of obstructive sleep apnea-hypopnea syndrome: A critical review," *J. Int. Neuropsych. Soc.*, vol. 10, no. 5, pp. 772–785, 2004.

[6] C. A. Kushida, M. R. Littner, T. Morgenthaler, C. A. Alessi, D. Bailey, J. Coleman Jr., L. Friedman, M. Hirshkowitz, S. Kapen, and M. Kramer, *et al.*, "Practice parameters for the indications for polysomnography and related procedures: An update for 2005," *Sleep*, vol. 28, no. 4, pp. 499–521, 2005.

[7] K. S. Park, S. H. Hwang, H. N. Yoon, and W. K. Lee, *et al.*, "Ballistocardiography for nonintrusive sleep structure estimation," in *Proc. IEEE 36th Annu. Int. Conf. Engineering in Medicine and Biology Soc.*, 2014, pp. 5184–5187.

[8] J. Haba-Rubio, G. Darbellay, F. R. Herrmann, J. G. Frey, A. Fernandes, J. M. Vesin, J. P. Thiran, and J. M. Tschopp, "Obstructive sleep apnea syndrome: Effect of respiratory events and arousal on pulse wave amplitude measured by photoplethysmography in NREM sleep," *Sleep Breath.*, vol. 9, no. 2, pp. 73–81, 2005.

[9] S. Ancoli-Israel, R. Cole, C. Alessi, M. Chambers, W. Moorcroft, and C. Pollak, "The role of actigraphy in the study of sleep and circadian rhythms. American academy of sleep medicine review paper," *Sleep*, vol. 26, no. 3, pp. 342–392, 2003.

[10] M. Sateia, K. Doghramji, P. Hauri, and C. Morin, "Evaluation of chronic insomnia," *Sleep*, vol. 23, no. 2, pp. 243–308, 2000.

[11] A. Sadeh, P. J. Hauri, D. F. Kripke, and P. Lavie, "The role of actigraphy in the evaluation of sleep disorders," *Sleep*, vol. 18, no. 4, pp. 288–302, 1995.

[12] Sleep Tracker. Last Access Date: Jan. 31, 2016. [Online]. Available: http://www.sleeptracker.com

[13] Fitbit. Last Access Date: Jan. 31, 2016. [Online]. Available: https://www.fitbit.com

[14] Sleep Cycle. Last Access Date: Jan. 31, 2016. [Online]. Available: http://www.sleepcycle.com

[15] M. Rofouei, M. Sinclair, R. Bittner, T. Blank, N. Saw, G. DeJean, and J. Heffron, "A non-invasive wearable neck-cuff system for real-time sleep monitoring," in *Proc. 2011 IEEE Int. Conf. Body Sensor Networks*, 2011, pp. 156–161.

[16] C.-W. Wang, A. Hunter, N. Gravill, and S. Matusiewicz, "Unconstrained video monitoring of breathing behavior and application to diagnosis of sleep apnea," *IEEE Trans. Biomed. Eng.*, vol. 61, no. 2, pp. 396–404, 2014.

[17] T. Hao, G. Xing, and G. Zhou, "isleep: Unobtrusive sleep quality monitoring using smartphones," in *Proc. 11th ACM Conf. Embedded Networked Sensor Systems*, 2013, p. 4.

[18] J. J. Liu, W. Xu, M.-C. Huang, N. Alshurafa, M. Sarrafzadeh, N. Raut, and B. Yadegar, "A dense pressure sensitive bedsheet design for unobtrusive sleep posture monitoring," in *Proc. IEEE Int. Conf. Pervasive Computing and Communications*, 2013, pp. 207–215.

[19] M. I. Skolnik, *Radar Handbook*. New York, NY, USA: McGraw-Hill, 1970.

[20] F. Wang, M. Skubic, M. Rantz, and P. E. Cuddihy, "Quantitative gait measurement with pulse-doppler radar for passive in-home gait assessment," *IEEE Trans. Biomed. Eng.*, vol. 61, no. 9, pp. 2434–2443, 2014.

[21] Y. S. Lee, P. N. Pathirana, T. Caelli, and R. Evans, "Doppler radar in respiratory monitoring: Detection and analysis," in *Proc. 2nd Int. Conf. Control Automation and Information Sciences*, 2013, pp. 199–203.

[22] C. Zheng, T. Hu, S. Qiao, Y. Sun, J. Huangfu, and L. Ran, "Doppler biosignal detection based time-domain hand gesture recognition," in *Proc. IEEE MTT-S Int. Microwave Workshop Series on RF and Wireless Technologies for Biomedical and Healthcare Applications*, 2013, p. 3.

[23] Y. Kim, S. Ha, and J. Kwon, "Human detection using doppler radar based on physical characteristics of targets," *IEEE Geosci. Remote Sensing Lett.*, vol. 12, no. 2, pp. 289–293, 2015.

[24] C. Gu, C. Li, J. Lin, J. Long, J. Huangfu, and L. Ran, "Instrument-based noncontact doppler radar vital sign detection system using heterodyne digital quadrature demodulation architecture," *IEEE Trans. Instrum. Meas.*, vol. 59, no. 6, pp. 1580–1588, 2010.

[25] B. Schleicher, I. Nasr, A. Trasser, and H. Schumacher, "Ir-uwb radar demonstrator for ultra-fine movement detection and vital-sign monitoring," *IEEE Trans. Microw. Theory Tech.*, vol. 61, no. 5, pp. 2076–2085, 2013.

[26] A. Lazaro, D. Girbau, and R. Villarino, "Techniques for clutter suppression in the presence of body movements during the detection of respiratory activity through uwb radars," *Sensors*, vol. 14, no. 2, pp. 2595–2618, 2014.

[27] D. Zito, D. Pepe, M. Mincica, F. Zito, A. Tognetti, A. Lanata, and D. De Rossi, "SoC CMOS UWB pulse radar sensor for contactless respiratory rate monitoring," *IEEE Trans. Biomed. Circuits Syst.*, vol. 5, no. 6, pp. 503–510, Dec. 2011.

[28] H. A. Kayyali, S. Weimer, C. Frederick, C. Martin, D. Basa, J. A. Juguilon, and F. Jugilioni, "Remotely attended home monitoring of sleep disorders," *Telemed. and e-Health*, vol. 14, no. 4, pp. 371–374, 2008.

[29] J. Kavanau, "Memory, sleep and the evolution of mechanisms of synaptic efficacy maintenance," *Neurosci.*, vol. 79, no. 1, pp. 7–44, 1997.

[30] N. Douglas, D. White, C. Pickett, J. Weil, and C. Zwillich, "Respiration during sleep in normal man," *Thorax*, vol. 37, no. 11, pp. 840–844, 1982.

[31] J. Wilde-Frenz and H. Schulz, "Rate and distribution of body movements during sleep in humans," *Percept. Motor Skills*, vol. 56, no. 1, pp. 275–283, 1983.

[32] A. Droitcour, V. Lubecke, J. Lin, and O. Boric-Lubecke, "A microwave radio for doppler radar sensing of vital signs," in *Proc. Dig. IEEE MTT-S Int. Microwave Symp.*, 2001, vol. 1, pp. 175–178.

[33] B. Lubecke, P.-W. Ong, and V. Lubecke, "10 ghz doppler radar sensing of respiration and heart movement," in *Proc. IEEE 28th Annu. Northeast Bioengineering Conf.*, 2002, pp. 55–56.

[34] M. Zakrzewski, H. Raittinen, and J. Vanhala, "Comparison of center estimation algorithms for heart and respiration monitoring with microwave doppler radar," *IEEE Sensors J.*, vol. 12, no. 3, pp. 627–634, 2012.

[35] N. A. Fox, C. Heneghan, M. Gonzalez, R. B. Shouldice, and P. de Chazal, "An evaluation of a non-contact biomotion sensor with actimetry," in *Proc. 29th Annu. Int. Conf. IEEE Engineering in Medicine and Biology Soc.*, 2007, pp. 2664–2668.

[36] P. De Chazal, N. Fox, E. O'Hare, C. Heneghan, A. Zaffaroni, P. Boyle, S. Smith, C. O'Connel, and W. T. Mcnicholas, "Sleep/wake measurement using a non-contact biomotion sensor," *J. Sleep Res.*, vol. 20, no. 2, pp. 356–366, 2011.

[37] C. Heneghan, C. Hanley, N. Fox, and P. De Chazal, "Apparatus, system, and method for monitoring physiological signs," Patent 8 562 526, Oct. 2013.

[38] C. Heneghan, C. Hanley, and P. De Chazal, "System and method for monitoring cardiorespiratory parameters," Patent 8 834 364, Sep. 2014.

[39] Y. Li, C. Gu, T. Nikoubin, and C. Li, "Wireless radar devices for smart human-computer interaction," in *Proc. IEEE 57th Int. Midwest Symp. Circuits and Systems*, 2014, pp. 65–68.

[40] J. Wang, X. Wang, L. Chen, J. Huangfu, C. Li, and L. Ran, "Noncontact distance and amplitude-independent vibration measurement based on an extended dacm algorithm," *IEEE Trans. Instrum. Meas.*, vol. 63, no. 1, pp. 145–153, 2014.

[41] E. Hughes, M. Lewis, and E. Reid, "The application of speech recognition techniques to radar target doppler recognition: A case study," in *Proc. IET Seminar High Resolution Imaging and Target Classification*, 2006, pp. 145–152.

[42] L. Liu, M. Popescu, M. Skubic, M. Rantz, T. Yardibi, and P. Cuddihy, "Automatic fall detection based on doppler radar motion signature," in *Proc. IEEE 5th Int. Conf. Pervasive Computing Technologies for Healthcare*, 2011, pp. 222–225.

[43] X. Long, P. Fonseca, J. Foussier, R. Haakma, and R. M. Aarts, "Sleep and wake classification with actigraphy and respiratory effort using dynamic warping," *IEEE J. Biomed. Health Inform.*, vol. 18, no. 4, pp. 1272–1284, 2014.

[44] X. Long, J. Foussier, P. Fonseca, R. Haakma, and R. M. Aarts, "Analyzing respiratory effort amplitude for automated sleep stage classification," *Biomed. Signal Process. Control*, vol. 14, pp. 197–205, 2014.

[45] M. Hall, E. Frank, G. Holmes, B. Pfahringer, P. Reutemann, and I. H. Witten, "The weka data mining software: An update," *ACM SIGKDD Explorations Newslett.*, vol. 11, no. 1, pp. 10–18, 2009.

[46] A. D. McGown, H. Makker, C. Elwell, P. G. Al Rawi, A. Valipour, and S. G. Spiro, "Measurement of changes in cytochrome oxidase redox state during obstructive sleep apnea using near-infrared spectroscopy," *Sleep*, vol. 26, no. 6, pp. 710–716, 2003.

[47] P. de Chazal, T. Penzel, and C. Heneghan, "Automated detection of obstructive sleep apnoea at different time scales using the electrocardiogram," *Physiol. Meas.*, vol. 25, no. 4, pp. 967, 2004.

[48] W. Webb and H. Agnew, "Sleep stage characteristics of long and short sleepers," *Science*, vol. 168, no. 3927, pp. 146–147, 1970.

[49] T. Rahman, A. T. Adams, R. V. Ravichandran, M. Zhang, S. N. Patel, J. A. Kientz, and T. Choudhury, "Dopplesleep: A contactless unobtrusive sleep sensing system using short-range doppler radar," in *Proc. ACM Int. Joint Conf. Pervasive and Ubiquitous Computing*, 2015, pp. 39–50.

[50] T. Rahman, A. T. Adams, M. Zhang, E. Cherry, B. Zhou, H. Peng, and T. Choudhury, "Bodybeat: A mobile system for sensing non-speech body sounds," in *Proc. 12th Annu. Int. Conf. Mobile Systems, Applications, and Services*, 2014, pp. 2–13.

[51] L. Samy, M.-C. Huang, J. J. Liu, W. Xu, and M. Sarrafzadeh, "Unobtrusive sleep stage identification using a pressure-sensitive bed sheet," *IEEE Sensors J.*, vol. 14, no. 7, pp. 2092–2101, 2014.

[52] X. Xu, F. Lin, A. Wang, C. Song, Y. Hu, and W. Xu, "On-bed sleep posture recognition based on body-earth mover's distance," in *Proc. IEEE Biomedical Circuits and Systems Conf.*, 2015, pp. 13–16.

[53] J. S. Carpenter and M. A. Andrykowski, "Psychometric evaluation of the pittsburgh sleep quality index," *J. Psychosom. Res.*, vol. 45, no. 1, pp. 5–13, 1998.

[54] M. A. Carskadon and W. C. Dement, *et al.*, "Normal human sleep: An overview," *Prin. Practice Sleep Med.*, vol. 2, pp. 16–25, 2000.

[55] D. Purves, G. J. Augustine, D. Fitzpatrick, L. C. Katz, A.-S. LaMantia, J. O. McNamara, and S. M. Williams, *et al.*, "Physiological changes in sleep states," *Neurosci.*, 2nd ed., Jul. 2001.

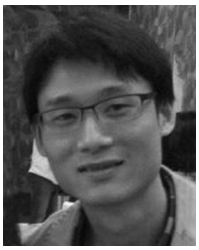

Feng Lin (S'11–M'15) received the B.S. degree from Zhejiang University, Hangzhou, China, in 2006, the M.S. degree from Shanghai University, Shanghai, China, in 2009, and the Ph.D. degree from the Department of Electrical and Computer Engineering, Tennessee Tech University, Cookeville, TN, USA, in 2015.

From 2009–2010, he worked for Alcatel-Lucent. Currently, he is a Research Scientist in the Department of Computer Science and Engineering, State University of New York (SUNY) at Buffalo, Buffalo, NY, USA. His research interests include signal processing, pattern recognition, embedded sensing, human-computer interface, wireless communications, and their applications in wireless health and biometrics.

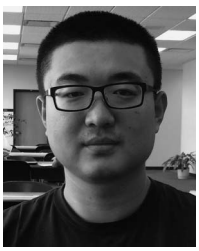

Yan Zhuang (S'14) received the B.S. degree from Tianjin Polytechnic University, Tianjin, China, and the M.S. degree from the State University of New York (SUNY) at Buffalo, Buffalo, NY, USA, in 2011 and 2014, respectively.

After graduation, he worked as a Research Associate at Embedded Sensing and Computing Lab in the Department of Computer Science and Engineering, SUNY–Buffalo. Currently, he is working toward the Ph.D. degree in computer engineering at the University of Virginia, Charlottesville, VA, USA. His interests are cyber-physical systems and body sensor networks.

Chen Song (S'14) received the B.S. degree in optic science and engineering from Fudan University, Shanghai, China, and the M.S. degree in electrical engineering from the State University of New York (SUNY) at Buffalo, Buffalo, NY, USA.

Currently, he is working toward the the Ph.D. degree in the Department of Computer Science, under the direction of Prof. Wenyao Xu, at SUNY–Buffalo. His research focuses on human-computer interaction, compressed sensing, and health-care and security in biomedical applications.

Aosen Wang (S'15) received the B.S. degree in electrical engineering from the University of Science and Technology of China, Hefei, China, in 2011.

Currently, he is working toward the Ph.D. degree in computer science and engineering at the State University of New York (SUNY) at Buffalo, Buffalo, NY, USA. He was with Vimicro as an Algorithm and Software Engineer. His research interests include low-power computer architecture and energy-efficient machine learning.

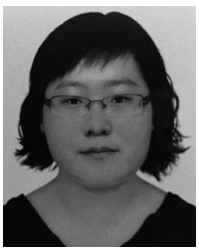

Yiran Li (S'12) received the B.S degree in electrical engineering from Southern Medical University, Guangzhou, China, and the M.S. degree in electrical and computer engineering from Texas Tech University, Lubbock, TX, USA, in 2009 and 2012, respectively.

Currently, she is working toward the Ph.D. degree in electrical and computer engineering at Texas Tech University. Her research interests include RFIC as well as analog IC circuit designs and applications.

Changzhan Gu (S'07–M'13) received the B.S. and M.S. degrees in electrical engineering from Zhejiang University, Hangzhou, China, in 2006 and 2008, respectively, the M.S. degree in electrical engineering from the University of Florida, Gainesville, FL, USA, in 2010, and the Ph.D. degree in electrical engineering from Texas Tech University, Lubbock, TX, USA, in 2013.

Currently, he is a member of the technical research team of Project Soli at Google Advanced Technology and Projects (ATAP) group, Mountain View, CA, USA. Prior to that, he was with Marvell Semiconductor Inc., where he was involved with wireless connectivity system-on-chip (SoC), and MaxLinear Inc., where he was involved with satellite TV tuner SoCs. His research interests include RF and microwave circuits/systems, RF SoCs, wireless sensing technologies, noncontact gesture sensing, and the emerging applications of RF/microwave.

Dr. Gu was the recipient of seven Best Paper Awards from IEEE-sponsored conferences as an author/coauthor. He was the recipient of the 2013 IEEE Microwave Theory and Techniques Society (MTT-S) Graduate Fellowship for Medical Applications, the 2013 Texas Tech Horn Professors Graduate Achievement Award, and the 2012 Chinese Government Award for Outstanding Self-Financed Students Abroad. He is an Area Editor for the *International Journal of Electronics and Communications*.

Changzhi Li (S'06–M'09–SM'13) received the B.S. degree in electrical engineering from Zhejiang University, Hangzhou, China, and the Ph.D. degree in electrical engineering from the University of Florida, Gainesville, FL, USA, in 2004 and 2009, respectively.

In the summers of 2007–2009, he was with Alereon Inc., Ausitn, TX, USA and then Coherent Logix Inc., Austin, TX, USA, where he was involved with ultrawideband (UWB) transceivers and software-defined radio, respectively. In 2009, he joined Texas Tech University, Lubbock, TX, USA, as an Assistant Professor, and became an Associate Professor in 2014. His research interests include biomedical applications of microwave technology, wireless sensors, and RF/analog circuits.

Dr. Li is an Associate Editor for the IEEE TRANSACTIONS ON CIRCUITS AND SYSTEMS I. He served as an Associate Editor for the IEEE TRANSACTIONS ON CIRCUITS AND SYSTEMS II in 2014 and 2015, and an Area Editor for the *International Journal of Electronics and Communications* from 2011 to 2013. He served as the TPC Cochair for the IEEE Wireless and Microwave Technology Conference (WAMICON) in 2012 and 2013. He received the Texas Tech Chancellor's Council Distinguished Research Award in 2015, the ASEE Frederick Emmons Terman Award in 2014, the IEEE-HKN Outstanding Young Professional Award in 2014, the Texas Tech Whitacre Research Award in 2014, the NSF Faculty Early CAREER Award in 2013, and the IEEE MTT-S Graduate Fellowship Award in 2008. He received nine best conference/student paper awards as author/advisor in IEEE-sponsored conferences.

Wenyao Xu (M'13) received the Ph.D. degree from the Electrical Engineering Department, University of California, Los Angeles, Los Angeles, CA, USA, in 2013.

Currently, he is an Assistant Professor in the Computer Science and Engineering Department, State University of New York (SUNY) at Buffalo, Buffalo, NY, USA. His research foci include embedded systems, computer architecture, wireless health, low-power technologies, and their applications in biomedicine, healthcare, and security. He has five licensed U.S. and international patents, and has authored more than 70 peer-reviewed journal and conference papers.

Dr. Xu received the Best Paper Award of the IEEE Conference on Implantable and Wearable Body Sensor Networks in 2013, and the Best Demonstration Award of ACM Wireless Health Conference in 2011.